UHASSELT
KNOWLEDGE IN ACTION

Maastricht University

Faculty of Medicine and Life Sciences
School for Life Sciences
Master of Biomedical Sciences

Master's thesis

Silent Messengers: Extracellular Vesicles as Mediators of Blood-Brain Barrier Breakdown in Metabolic Dysfunction-Associated Steatohepatitis

Céline Meynen

Thesis presented in fulfillment of the requirements for the degree of Master of Biomedical Sciences, specialization Molecular Mechanisms in Health and Disease

SUPERVISOR :

Prof. dr. Bieke BROUX

MENTOR :

Mevrouw Daphne LINTSEN

2024
2025

Transnational University Limburg is a unique collaboration of two universities in two countries: the University of Hasselt and Maastricht University.

UHASSELT
KNOWLEDGE IN ACTION

www.uhasselt.be
Universiteit Hasselt
Campus Hasselt:
Martelarenlaan 42 | 3500 Hasselt
Campus Diepenbeek:
Agoralaan Gebouw D | 3590 Diepenbeek

UHASSELT
KNOWLEDGE IN ACTION

Maastricht University

Faculty of Medicine and Life Sciences
School for Life Sciences
Master of Biomedical Sciences

Master's thesis

Silent Messengers: Extracellular Vesicles as Mediators of Blood-Brain Barrier Breakdown in Metabolic Dysfunction-Associated Steatohepatitis

Céline Meynen

Thesis presented in fulfillment of the requirements for the degree of Master of Biomedical Sciences, specialization Molecular Mechanisms in Health and Disease

SUPERVISOR :

Prof. dr. Bieke BROUX

MENTOR :

Mevrouw Daphne LINTSEN

Silent Messengers: Extracellular Vesicles as Mediators of Blood-Brain Barrier Breakdown in Metabolic Dysfunction-Associated Steatohepatitis

Céline Meynen[1], Daphne Lintsen[1], and Prof. Dr. Bieke Broux[1]

[1]CBN lab, Biomedical Research Institute, Universiteit Hasselt, Campus Diepenbeek, Agoralaan Gebouw C - B-3590 Diepenbeek

*Running title: *Liver EVs and BBB Integrity in MASH*

To whom correspondence should be addressed: Prof. dr. Bieke Broux, Tel: +3211269254; Email: bieke.broux@uhasselt.be

Keywords: Liver, MASH, inflammation, extracellular vesicles, blood-brain barrier, inter-organ crosstalk

---

ABSTRACT

Metabolic dysfunction-associated steatohepatitis (MASH) is a progressive liver disease increasingly recognized for its impact on extrahepatic tissues, including effects on the central nervous system. Notably, MASH has been shown to compromise the blood-brain barrier (BBB) integrity, potentially contributing to neuroinflammation. However, the exact mechanisms underlying BBB impairment in the context of MASH remain elusive. Therefore, this study investigates whether liver-derived extracellular vesicles (EVs) play a role in mediating this BBB dysfunction. To model MASH pathology, mice were fed a high-fat, high-glucose diet for 15, 20, or 25 weeks. Liver-derived EVs were subsequently isolated and characterized. Analysis of brain tissue from MASH mice revealed transcriptional changes linked to BBB breakdown, leukocyte adhesion, and inflammation, along with increased parenchymal IgG accumulation, indicative of barrier leakage. Furthermore, *in vitro* exposure of brain endothelial cells to MASH-derived EVs reduced barrier integrity, as evidenced by decreased transendothelial electrical resistance and downregulation of VE-Cadherin. Simultaneously, VCAM-1 expression was elevated, further supporting endothelial activation and compromised barrier function upon exposure to MASH liver-derived EVs. These effects were most pronounced at 25 weeks, suggesting a progressive relationship between disease severity and BBB impairment. Collectively, these findings point to a pathological role for liver-derived EVs in mediating BBB dysfunction in MASH.

INTRODUCTION

The liver is a metabolically active organ essential for maintaining whole-body homeostasis (1). It plays a central role in the energy metabolism, nutrient storage, hormone regulation, and detoxification of both endogenous and exogenous compounds (1, 2). The liver is highly specialized and composed of both parenchymal and non-parenchymal cells (1). Hepatocytes, the primary parenchymal cells, are responsible for the bulk of the liver's metabolic, anabolic, and catabolic functions (1). In addition, the liver contains a variety of non-parenchymal cells, including Kupffer cells, specialized resident macrophages; liver sinusoidal endothelial cells; and hepatic stellate cells (2). While these cells contribute to homeostatic processes such as filtration and extracellular matrix maintenance, they can also play essential roles in the liver's immunological functions (1, 3-5). Particularly under inflammatory or pathological conditions, the liver acts as an immunological organ by initiating immune responses, and producing cytokines and chemokines that can influence both local and systemic inflammation (1-5).

The architecture and function of the liver can be disrupted by chronic metabolic stressors (e.g., insulin resistance, obesity, diabetes), leading to the development of metabolic dysfunction-associated steatotic liver disease (MASLD), formerly known as non-alcoholic fatty liver disease (6-8). MASLD is characterized by excessive lipid accumulation in hepatocytes, affecting approximately 25% of the global population (6, 9). It is strongly associated with comorbidities such as insulin resistance, cardiovascular disease, dyslipidemia, obesity, and type 2 diabetes mellitus, which are all features of the metabolic syndrome (6). The prevalence of MASLD increases with age, obesity, and lack of physical activity (10). In these high-risk populations, the prevalence can climb up to 60% (10). Due to hepatic liver accumulation, oxidative stress, and organelle dysfunction, MASLD can progress to metabolic dysfunction-associated steatohepatitis (MASH), formerly known as non-alcoholic steatohepatitis (NASH), a more severe form involving hepatocellular injury, inflammation, and varying degrees of fibrosis (6, 11). Approximately 20% of patients with MASLD will develop MASH, and therefore, it is estimated to affect 1.5–6.45% of the global population (6, 12-15). MASH may eventually lead to cirrhosis and hepatocellular carcinoma if left untreated (6, 12, 13).

During the disease progression of MALSD to MASH, the inflammation and fibrosis of the liver lead to hepatocyte ballooning, infiltrating leukocytes, and thereby, overproduction of pro-inflammatory cytokines and reactive oxygen species (ROS) (16, 17). The overproduction of ROS is due to the increasing number of Kupfer cells present in MASH (16). Additionally, the triglycerides accumulating in the liver can lead to lipotoxicity, which induces the production of ROS and lipid peroxidation (16). These processes contribute to hepatocyte dysfunction and cell death, either through apoptosis or necrosis (16). The chronic inflammatory state of the liver not only impairs its function but may also have distant consequences, including effects on the central nervous system (CNS) (18-20).

Emerging evidence suggests a link between MASLD/MASH and neurological dysfunction, including cognitive impairment and neuroinflammation due to the alterations happening in MASH (18-20). The blood-brain barrier (BBB) serves as a critical interface between the CNS and the peripheral circulation, maintaining brain homeostasis by tightly regulating the passage of molecules, cells, and ions (21). Composed primarily of endothelial cells connected by junctional complexes such as tight junctions, gap junctions, and adherens junctions, the BBB is highly selective (21). In addition to endothelial cells, the BBB is comprised of pericyte and astrocyte end feet that combine their efforts to maintain the integrity of the BBB (21). However, its integrity can be compromised in pathological conditions, including MASH (18, 19). When the integrity is compromised, its selective permeability is disrupted, allowing the uncontrolled entry of molecules, leukocytes, toxins, and potentially harmful substances into the CNS (22). This can lead to neuroinflammation, oxidative stress, and damage to neuronal tissue, contributing to the progression of various neurological disorders (22). Recent studies have demonstrated that MASH is associated with a decreased expression of Zona Occludens-1 (ZO-1) and Claudin 5 (CLDN5) which are

important components of tight junctions; increased microglial activation; increased expression of endothelial activation markers such as vascular cell adhesion molecule 1 (VCAM-1) and intercellular adhesion molecule 1 (ICAM-1); and increased permeability of the BBB (18, 19, 23, 24). Together, these findings support the contribution of MASH to BBB dysfunction and highlight the need to further investigate the mechanisms linking liver pathology to neuroinflammation (18-20, 23, 24).

Despite this growing body of evidence linking liver pathology to neuroinflammation and BBB disruption, the exact mechanisms underlying the impairment of BBB integrity remain poorly understood. Exploring these mechanisms is crucial for identifying potential therapeutic strategies for both liver-related and neurological disorders. One potential influencing factor is inter-organ crosstalk, which may be mediated by extracellular vesicles (EVs) from peripheral organs and affect BBB integrity (25). EVs are nano- to micro-sized membranous particles that can be released by virtually all cells in the body (25). Different subtypes of EVs can be distinguished based on their size and origin (25). They originate either from the cell membrane directly (microvesicles) or form within the cell, subsequently being taken up by a multivesicular body (MVB) and excreted from the cell via membrane fusion (exosomes) (25). They all consist of a lipid bilayer and cargo, which can include: DNA, RNA, lipids, and proteins (25). These EVs can interact with near and distant cells by releasing their cargo into the cell via endocytosis or fusion or by interacting with their surface proteins and triggering the activation of intracellular cascades (Fig. 1) (26). A widely used approach to identify and characterize EVs,

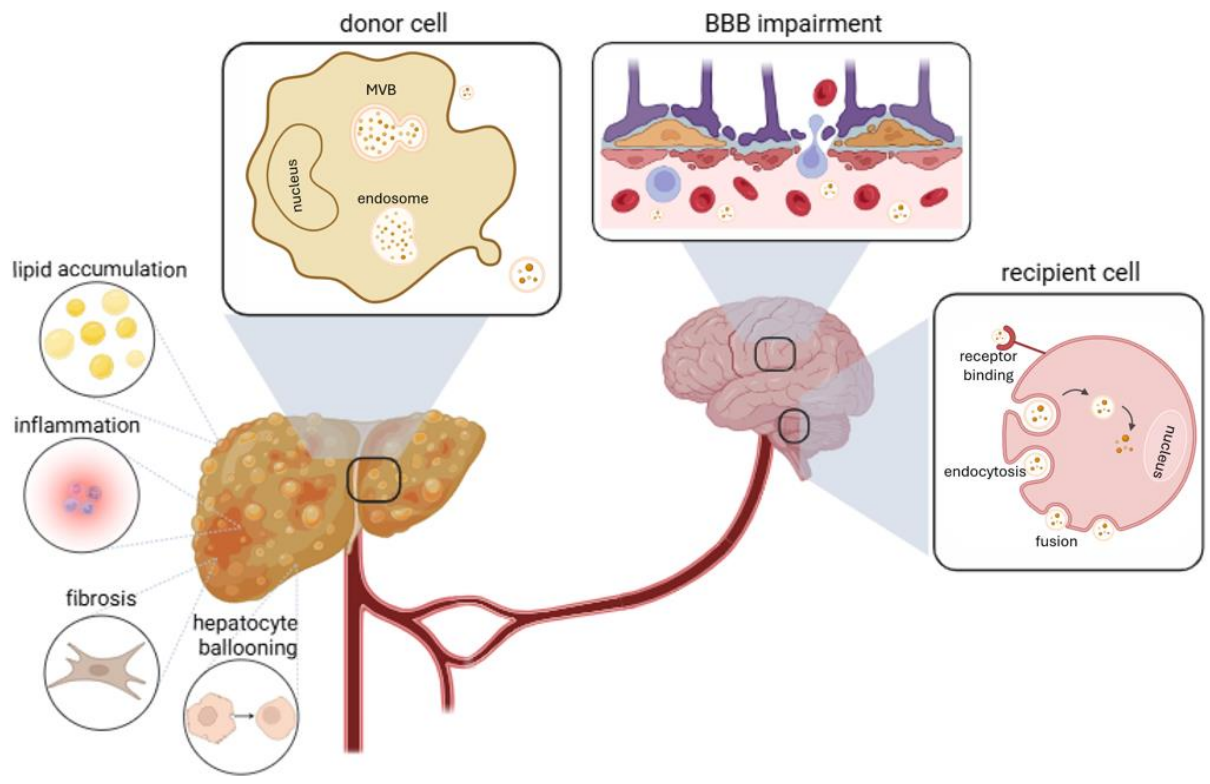

Fig. 1 – Schematic overview of EV-mediated inter-organ crosstalk. A MASH liver, characterized by steatosis, inflammation, hepatocellular ballooning, and fibrosis, releases EVs from donor cells into circulation. These EVs may interfere with the BBB and could be taken up by recipient cells, potentially contributing to neuropathological changes.
BBB: blood-brain barrier, EV: extracellular vesicle, MASH: metabolic dysfunction-associated steatohepatitis, MVB: multivesicular body.

particularly exosomes, is the detection of tetraspanins, which include CD9, CD63, and CD81 (25, 27). These transmembrane proteins are commonly enriched on the surface of exosomes and play a functional role in vesicle biogenesis, membrane organization, and mediating interactions with target cells (27). Their presence serves as a hallmark of exosome isolation and supports their involvement in targeted intercellular communication (27). The liver, as a highly metabolic organ, also secretes EVs that can reflect the liver's pathological state (28). In obesity and related metabolic disorders, circulating EVs are known to carry a diverse array of bioactive molecules, including cytokines, lipids, and microRNAs, which can modulate the function of distant tissues (29). Several studies have demonstrated that adipose and hepatic tissue release EVs capable of promoting systemic inflammation and insulin resistance, indicating their role in metabolic dysfunction (28-31). In the context of MASH, liver-derived EVs have been shown to carry inflammatory and fibrogenic signals, contributing to hepatic injury and fibrotic progression (32, 33). More recently, there has been growing interest in how these vesicles might influence extrahepatic organs.

Emerging evidence suggests that EVs can cross the BBB or modulate its function (34, 35). Studies have shown that EVs released during systemic inflammation or metabolic diseases can affect BBB permeability and alter the behavior of brain-resident cells, such as microglia and astrocytes (36). This raises the possibility that liver-derived EVs, particularly in the context of MASH, may exert a direct influence on the BBB and CNS. However, the mechanisms by which EVs contribute to BBB disruption, especially in the context of chronic metabolic liver disease, remain unclear.

Therefore, this study aims to investigate whether EVs derived from the liver of mice with MASH negatively impact the integrity of the BBB. Consequently, we hypothesize that EVs derived from murine MASH-affected liver cells may impair BBB integrity, potentially by disrupting the tight junction complexes, thereby establishing a link between liver pathology and neurological dysfunction. By characterizing these EVs and assessing their effects on the BBB, this study seeks to uncover novel mechanisms underlying MASH-induced cerebrovascular dysfunction.

EXPERIMENTAL PROCEDURES

Mice – 8-week-old female wild-type C57BL/6J mice were divided into two groups: one group was fed a Gubra-Amylin NASH (GAN) diet consisting of 40% fat, 20% fructose, 10% sucrose, and 2% cholesterol to induce MASH, while the control group was fed a matched-control diet with 13% fat, low sugar, and low cholesterol levels. Mice were placed on these diets for 15, 20, or 25 weeks. At the end of the respective dietary periods, mice were exposed to CO_2 after which liver perfusion was performed using phosphate-buffered saline (PBS) with heparin. The livers were harvested, and the brains were then carefully isolated and immediately snap-frozen in liquid nitrogen for further analysis. Additionally, blood, visceral adipose tissue (vAT), and subcutaneous adipose tissue (scAT) were collected. All animal procedures were approved by the Dierexperimentencommissie UM.

qPCR – RNA was isolated using the RNeasy Mini Kit (250) (74106, Qiagen, Germany) following the manufacturer's instructions, including an initial lysis step with QIAzol. RNA concentration was determined using a Nanodrop 2000/2000c spectrophotometer (Thermo Fisher, USA), with absorbance measured at 260 and 280 nm. Additionally, the RNA concentration was adjusted to 50 ng/µL in RNase-free water with qScript (1:5), and cDNA synthesis was performed under the following conditions: 25°C for 5 min, 42°C for 30 min, 85°C for 5 min, at 4°C. Subsequently, cDNA samples were diluted 1:10 in RNase-free water. Primers were diluted likewise (Table S1). Reactions contained SYBR Green (1:2) (4385612, Thermo Fisher), RNase-free water (8:50), and each of forward and reverse primers (3:100). An equal amount of cDNA (1:4) was added and amplification was done on a QuantStudio system (Thermo Fisher, USA) under the following conditions: 95°C for 20 sec, followed by 40 cycles of 95°C for 3 sec and 60°C for 30 sec, followed by 95°C for 15 sec, 60°C for 60 sec, and 95°C for 15 sec.

Immunohistochemistry - Whole brains of MASH-diet fed mice and control-diet fed mice were cryosectioned (10 µM thickness), after which sections were fixed in ice-cold acetone for 10 min. After drying, the sections were washed in PBS, and blocked with 10% protein block (Dako, Agilent, USA) for 30 min at room temperature (RT). Rabbit anti-mouse laminin in PBS (1:2000, ab30320, abcam, UK) was added overnight at 4°C. Sections were washed and incubated for 1h at RT in the dark with secondary antibodies diluted in 10% protein block: goat anti-rabbit Alexa Fluor 488 (1:600, #A-11008, Thermo Fisher, USA) and donkey anti-mouse IgG (H+L) Alexa Fluor 488 (1:800, #A-21202, Thermo Fisher, USA). DAPI (1:10,000) was used for nuclear staining. To reduce autofluorescence, sections were treated with 0.3% Sudan Black (Merck, Germany) in 70% ethanol for 10 min, followed by multiple washing steps in 70% ethanol and PBS. Finally, slides were mounted with fluorescent mounting medium and sealed with coverslips. Microscopic analysis was performed using Leica DM2000 LED (Leica Microsystems, Germany), and quantification was performed using ImageJ (Version 1.51).

Size exclusion chromatography (SEC) – Half of the right lobe of the liver was used for EV isolation. Therefore, liver cells were isolated by mechanical disruption, and the resulting cell suspension was filtered through 70 µm nylon strainers into RPMI 1640 medium (Gibco, Thermo Fisher, USA) and centrifuged at 50 g for 10 min at 4°C. The supernatant was processed through a series of centrifugation steps at 300 g, 2000 g, and 10,000 g at 4°C. The supernatant was concentrated using 100 kDa filters (Amicon, Merck Millipore, Germany). Concentrated media samples were loaded on a 70 nm SEC-column (IZON science, New Zealand) and EVs were isolated according to the manufacturer's instructions. For each sample, ten fractions of 1 mL were collected in PBS.

Nanoparticle tracking analysis (NTA) – NTA (ZetaView, Particle Metrix, Germany) was used to determine the EV's size and concentration. The pre-acquisition parameters were set at: a temperature of 23.5°C, 11 measurement positions, 60 frames per second, scatter of 80, shutter of 100, and frame rate of 30. All samples were individually diluted in PBS to achieve the optimal concentration range for detection.

Western blot – EV samples were mixed with 1× Laemmli sample buffer containing 5% β-mercaptoethanol and denatured at 95°C for 5 min. Proteins were separated on a 12% SDS-PAGE gel at 200V and transferred onto a PVDF membrane at 0.15 A. Following transfer, the membrane was blocked for 1 h in Tris-buffered saline with 0.1% Tween (TBS-T) supplemented with 5% Marvel. The membrane was then incubated overnight with primary antibodies in TBS-T, including anti-CD9 (1/1000, #10626D, Thermo Fisher, USA), anti-CD63 (1/1000, EPR21151, abcam, UK), anti-CD81 (1/1000, #10630D, Thermo Fisher, USA), anti-Alix (1/500, #MA1-83977, Thermo Fisher, USA), anti-ApoE (1/1000, # 701241, Thermo Fisher, USA), and anti-BAX (1/1000, #14-6997-82, Thermo Fisher, USA). After incubation, the blot was washed at least three times with TBS-T before incubation with horseradish peroxidase-conjugated secondary antibodies in TBS-T + 5% Marvel (goat anti-mouse (1/1000, Agilent, USA) or goat anti-rabbit (1/1000, Agilent, USA)) diluted 1:1,000 for 1 h. The membrane was washed at least three times with TBS-T. Protein detection was performed using an enhanced chemiluminescence kit (Thermo Fisher, USA), and signals were visualized using chemiluminescent Amersham TM Imager 680 (Thermo Fisher, USA).

Human cerebral microvascular endothelial cells (hCMEC/D3) cell culture – hCMEC/D3 cells were cultured on collagen-coated flasks (1:45 in PBS, ≥2 h at 37°C) (C3867-1VL, rat, Sigma-Aldrich, USA) in EGM2-MV medium (Lonza, Switzerland) supplemented with 5 ng/mL VEGF, 5 ng/mL hEGF, 1 ng/mL hFGF-B, 15 ng/mL R3-IGF, 50 µg/mL ascorbic acid, 1.4 µM hydrocortisone, 10 µg/mL gentamicin, 1 µg/mL amphotericin, and 2.5% FBS. Cells were maintained at 37°C in 5% CO_2. For treatment, confluent monolayers were exposed for 24 h to serum-reduced EBM2 medium with 1 ng/mL hFGF-B, 10 µg/mL gentamicin, 1µg/mL amphotericin, and 0.25% FBS, supplemented with control or MASH-liver derived EVs (1:10). EV preparations were filtered (0.2 µm) before addition.

Flow cytometry – Treated hCMEC/D3 cells were stained with anti-CD54 PE-Dazzle 594 (1:500, HA58, 353117, BioLegend, USA), anti-CD106 APC (1:250, STA, 305810, BioLegend, USA), and anti-CD144 FITC (1:10, 560411, BD Biosciences, USA). Quantification was performed on a Fortessa flow cytometer (BD Biosciences, USA), and data were analysed with FlowJo software (V10.10.0, BD Biosciences, USA).

Transendothelial electrical resistance (TEER) – hCMECs/D3 cells were seeded on a collagen type I (C3867-1VL, rat, Sigma-Aldrich, USA)-coated 96-well plate (CytoView-Z96, Z96-IMP-96B, AXION biosystems, The Netherlands). Once cells reached confluency, they were treated using the following conditions: untreated, TNF-α + INF-γ (1:1000), MASH liver-derived EVs with TNF-α + INF-γ, and control liver-derived EVs with TNF-α + INF-γ. TEER was measured at a frequency of 1, 10, and 43.5 kHz on the Maestro Z (AXION Biosystems, The Netherlands).

Statistical analyses – Data were analysed using GraphPad Prism v10.4.0 (GraphPad Software Inc., USA) and are expressed as mean ± standard error of the mean (SEM). The Grubbs' test was performed to identify outliers. The Shapiro-Wilk test was applied to assess the normality of the data. The Mann-Whitney U or Kruskal-Wallis test were performed for non-normally distributed data. A p-value of less than 0.05 was considered statistically significant, with significance levels indicated as: *p < 0.05, **p < 0.01, and ***p < 0.001.

RESULTS

MASH induces hepatic and adipose tissue alterations during disease progression – To model MASH in a murine model, a dietary intervention using the GAN diet was implemented for 15, 20, or 25 weeks. To investigate the hepatic and extrahepatic effects of MASH, mice were fed the GAN diet for these periods, while control animals received a matched-control diet. During the duration of the diet, all mice gained body weight. After 25 weeks on the GAN diet, this increase in mice with MASH was significant compared to controls (p = 0.0317) (Fig. 2A). Liver weight was significantly elevated at both 20 weeks (p = 0.0022) and 25 weeks (p = 0.0159), reflecting the hepatic impact of the diet (Fig. 2B). vAT weight did not differ significantly between groups (Fig. 2C). In contrast, scAT weight was significantly increased at 25 weeks (p = 0.0476) in the MASH group (Fig. 2D), suggesting selective expansion of scAT rather than vAT. The GAN diet successfully induced a MASH-like phenotype, characterized by clear pathological changes at both hepatic and adipose tissue levels, providing a relevant model to study downstream effects such as BBB dysfunction.

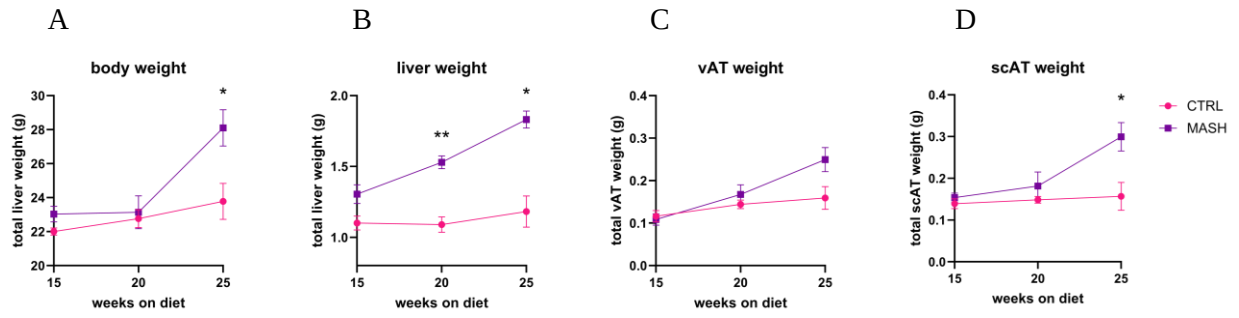

Fig. 2 – **Body, liver and scAT weight increases as MASH progresses.** Mice were subjected to either CTRL or GAN diet for 15, 20, or 25 weeks (n = 6 for 15 weeks, n = 5 for 20 and 25 weeks per group). Total body weight (A), total liver weight (B), total vAT weight (C), and total scAT (D) weight were measured. A Mann-Whitney U-test was performed and the data are presented as mean ± SEM, *: p < 0.05, **: p < 0.01.
CTRL: control, MASH: metabolic dysfunction-associated steatohepatitis, scAT: subcutaneous adipose tissue, vAT: visceral adipose tissue.

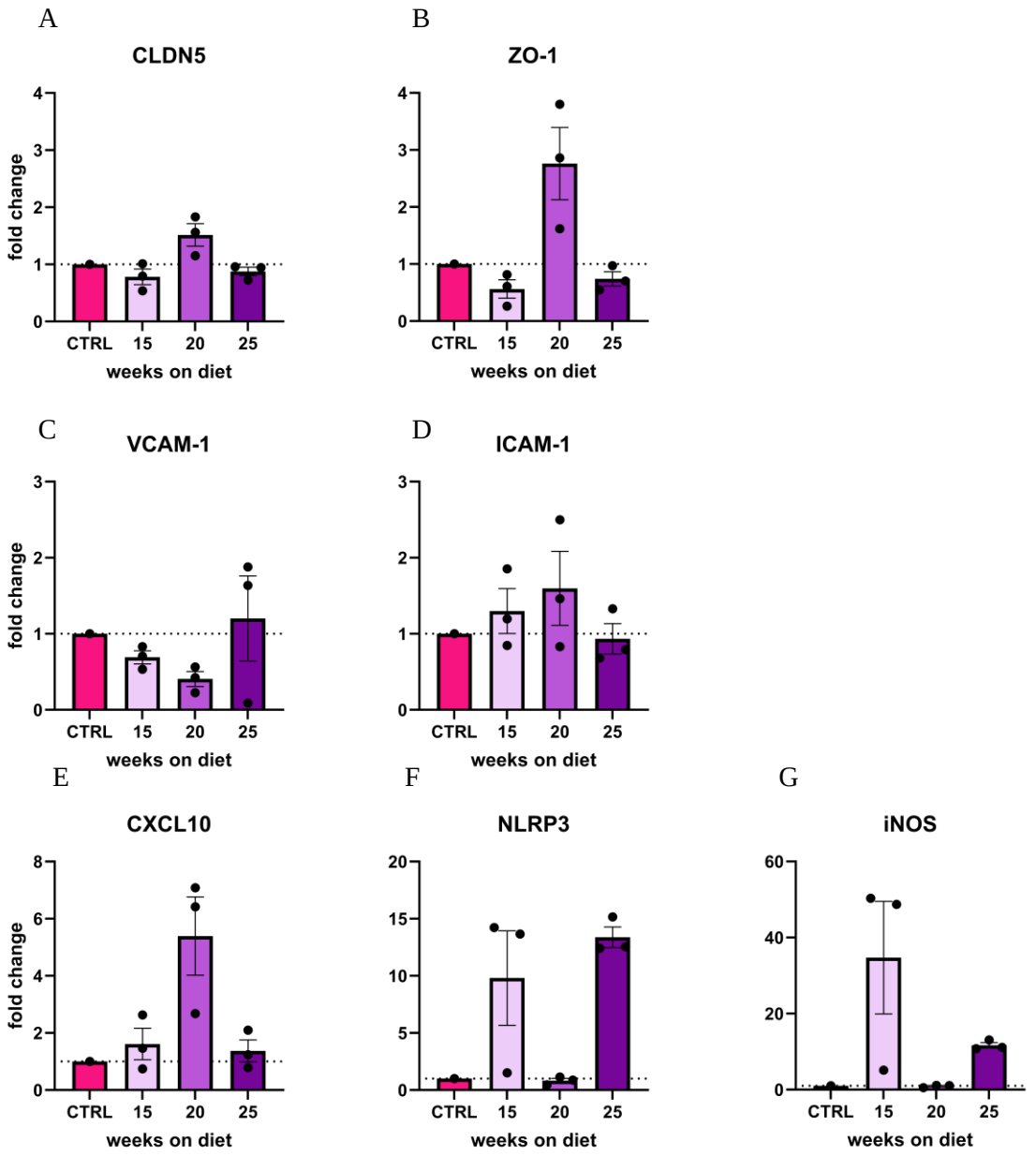

Fig. 3 – MASH induces gene expression changes indicative of BBB impairment and neuroinflammatory activation.

qPCR was performed on whole brain lysates to evaluate genes associated with tight junction integrity (CLDN5 (A), ZO-1 (B)), endothelial activation (VCAM-1 (C), ICAM-1 (D)), chemokine signalling (CXCL10 (E)), inflammasome activation (NLRP3 (F)), and microglial activation (iNOS (G)). Data are shown as fold change normalized to housekeeping genes and CTRL. A Kruskal-Wallis test was performed (n = 3/group), and the data are presented as mean ± SEM.

BBB: blood-brain barrier, CLDN5: Claudin-5, CTRL: control, CXCL10: C-X-C motif chemokine ligand 10, ICAM-1: intercellular adhesion molecule-1, iNOS: inducible nitric oxide synthase, MASH: metabolic dysfunction-associated steatohepatitis, NLRP3: NOD-like receptor family pyrin domain containing 3, VCAM-1: vascular cell adhesion molecule-1, ZO-1: zona occludens 1.

Gene expression trends suggest BBB dysregulation and inflammatory shifts in MASH – To explore potential effects of MASH on BBB integrity and neuroinflammatory signaling, qPCR was performed on brain tissue from mice exposed to the GAN diet for 15, 20, or 25 weeks. Although none of the observed changes reached statistical significance, likely due to limited sample size, several consistent trends were noted that may point toward MASH-associated cerebrovascular alterations. Markers associated with BBB structure showed modest variations. CLDN5 and ZO-1 expression fluctuated over time, with a slight tendency to decrease at 25 weeks, indicating potential alterations in tight junction integrity during MASH progression (Fig. 3A-B). In terms of vascular inflammation, VCAM-1 and ICAM-1 expression trended upward with MASH progression (Fig. 3C-D). These markers are involved in leukocyte adhesion and may reflect endothelial activation. Pro-inflammatory markers, including C-X-C motif chemokine ligand 10 (CXCL10), NOD-like receptor family pyrin domain containing 3 (NLRP3), and inducible nitric oxide synthase (iNOS) also demonstrated increased expression in MASH-exposed animals at specific timepoints, most notably CXCL10 at 20 weeks and NLRP3 at 25 weeks, suggesting a possible shift toward a more inflammatory CNS environment (Fig. 3E-G).

Immunohistochemistry indicates increased BBB leakage in MASH mice – To evaluate the permeability of the BBB in MASH, immunohistochemistry staining for immunoglobulin G (IgG) and laminin was

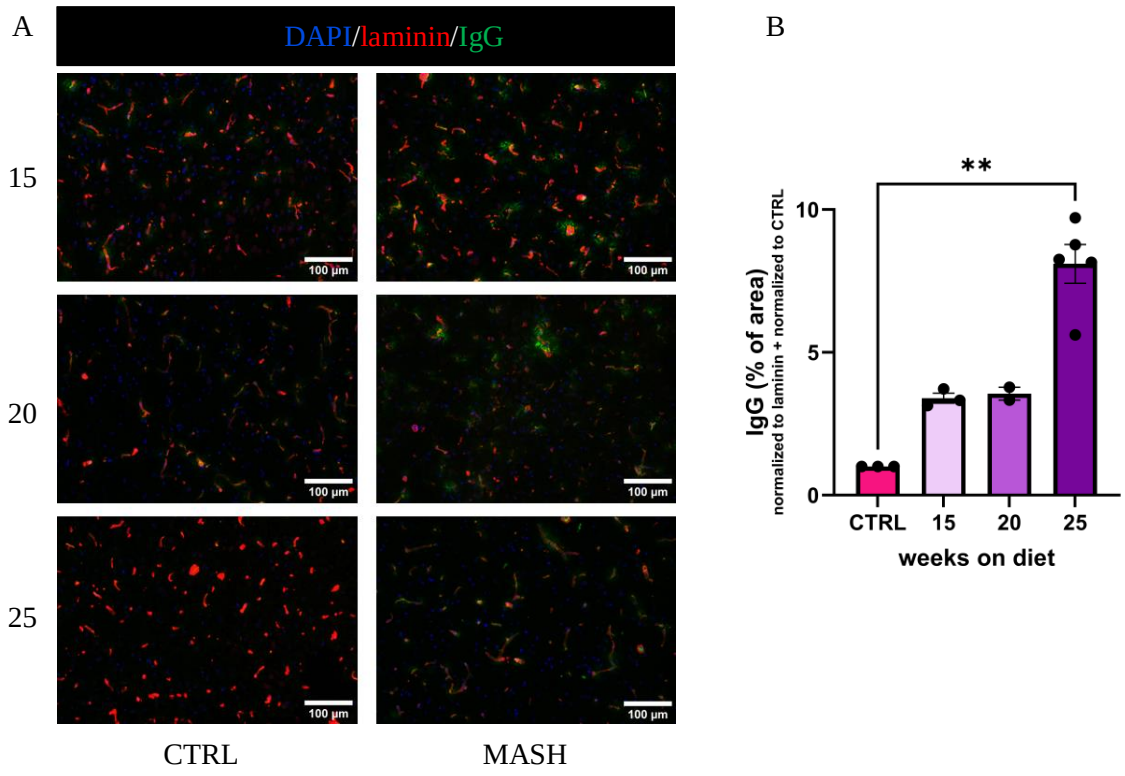

Fig. 4 – Immunohistochemical staining of whole-brain sections shows increased BBB leakage in MASH mice.
Whole-brain coronal sections were stained for endogenous IgG (green), laminin (red), and nuclei (DAPI, blue) at 15, 20, and 25 weeks, indicating progressive BBB leakage. Quantification of IgG fluorescence area, IgG was normalized to laminin and CTRL. A Kruskal-Wallis test was performed, n = 3 (15 weeks), n = 2 (20 weeks), n = 4 (25 weeks); the data are presented as mean ± SEM, **: $p < 0.01$. Scale bar = 100 µm, 20x magnification.
BBB: blood-brain barrier, CTRL: control, DAPI: 4', 6-diamidino-2-phenylindole, IgG: immunoglobulin G, MASH: metabolic dysfunction-associated steatohepatitis.

performed on whole-brain sections of control and MASH mice at 15, 20, and 25 weeks of dietary intervention (Fig. 4A). Laminin was used to visualize the vasculature, while extravascular IgG served as a marker of BBB permeability. Across MASH conditions, a progressive increase in parenchymal IgG signal was observed, most notably at 25 weeks, suggesting enhanced BBB leakage at later disease stages (Fig. 4B). Milder increases were also visible at 15 and 20 weeks. Quantification of IgG area supported this trend, though the differences did only reach statistical significance at 25 weeks of diet ($p = 0{,}0088$) (Fig. 4B). These results align with other findings of endothelial barrier impairment in the MASH model and point toward a potential relationship between prolonged disease state and compromised BBB function.

EV profiling reveals fraction four as EV-rich, dominated by small EVs – Half of the right liver lobe was incubated *ex vivo*, allowing liver cells to spontaneously release EVs into the surrounding medium, referred to as conditioned medium. This medium was subsequently concentrated and subjected to SEC, which separates particles based on size. Ten sequential fractions of 1 mL were collected per sample and analysed by NTA to characterize EV concentration and size distribution. NTA of ten distinct SEC fractions revealed that particle yield peaked consistently in fractions four to six across all groups, indicating that EV isolation using SEC was successful (Fig. 5A-B). Overall, fraction four exhibited the highest particle concentration and was therefore selected for downstream analyses (Fig. 5A-B). Size distribution analysis of this fraction demonstrated no major differences between control and MASH groups

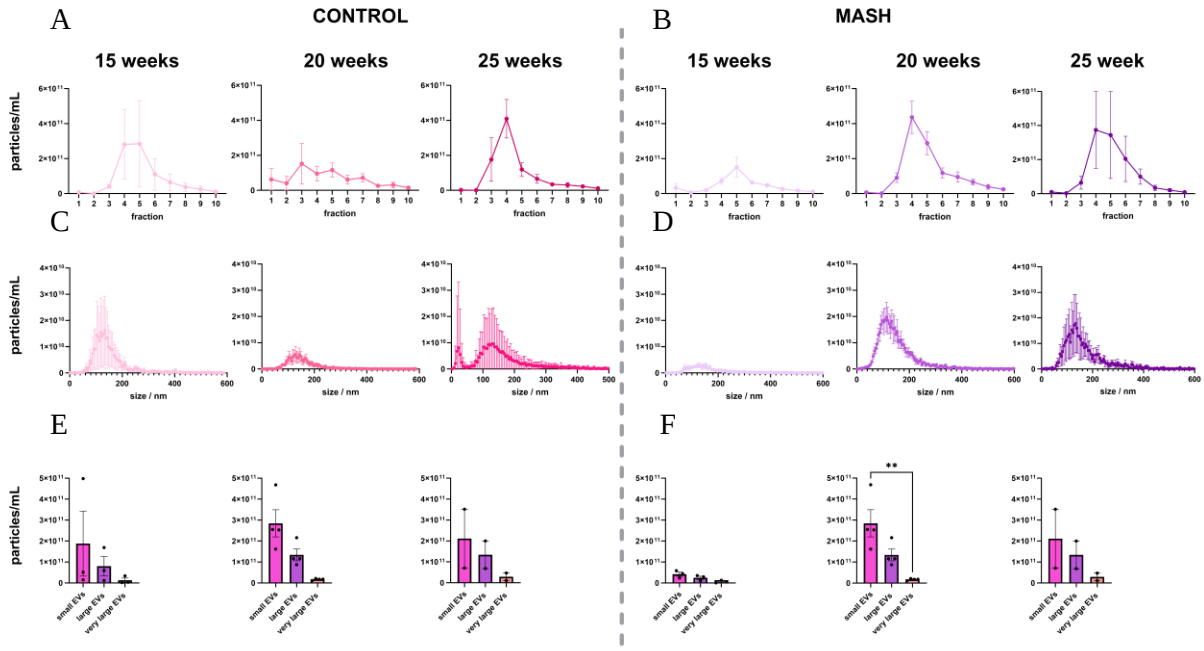

Fig. 5 – Liver-derived EVs are primarily detected in SEC fractions four to six and consist mainly of small vesicles determined by NTA.
A-B: EV yield per SEC-isolated fraction (1–10) from whole liver of CTRL (A) and MASH (B) mice following 15, 20, or 25 weeks of diet. C-D: Size distribution profiles of particles in fraction four, representing the EV-rich peak, for CTRL (C) and MASH (D) samples. E–F: Quantification of particle concentrations in three size-defined EV subpopulations (small: <150 nm; large: 150–300 nm; very large: >300 nm) across all time points of CTRL (E) and MASH (F) EVs. Statistical analysis by Kruskal-Wallis test; n = 12/group (A–D), 15 weeks: n = 3/group, 20 weeks: n = 4, 25 weeks: n = 2 (E–F). Data presented as mean ± SEM, **: $p < 0.01$.
CTRL: control, MASH: metabolic dysfunction-associated steatohepatitis, NTA: nanoparticle tracking analysis, SEC: size exclusion chromatography.

across all time points, with an average peak size of 123.0 ± 2.9 nm (Fig. 5C–D, Fig. S1A). When EVs were categorized into small (<150 nm), large (150–300 nm), and very large (>300 nm) subpopulations, small EVs were found to dominate in all groups (Fig. 5E–F). A statistically significant difference between small and very large EVs was observed specifically in the 20-week MASH group ($p = 0.007$), indicating a relative enrichment of small EVs under MASH conditions at this stage. Notably, a similar trend favoring small EVs was present across all groups, though not statistically significant. Lastly, direct comparison of particle concentrations in fraction four between control and MASH conditions at each time point revealed no significant differences (Fig. S1B), suggesting that total EV yield remains relatively stable, regardless of the diet the mice were exposed to. To further validate the efficiency of the SEC-based EV isolation, a BCA protein assay was performed on all ten collected fractions of mice that were on the diet for 20 weeks. This analysis revealed an upward trend in total protein content across the fractions, with the highest levels consistently detected in the later-eluting fractions (fractions seven to ten) (Fig. S2). This pattern supports the expected separation profile of SEC, where smaller particles, such as free proteins, elute later than larger vesicular particles.

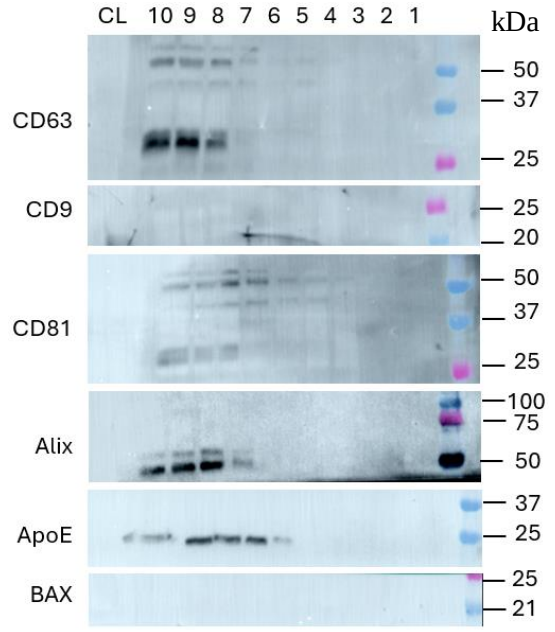

Fig. 6 – Western blot analysis reveals the presence of EV markers in fractions eight to ten, the presence of lipoprotein contamination, and the absence of common apoptotic bodies in at 25 weeks of MASH diet.
EV markers CD63, CD81, and Alix were detected in fractions eight to ten, while CD9 was absent. ApoE was present in cell lysate and fractions eight to ten, BAX was absent. Cell lysates were taken along as a control. CL: cell lysate, kDa: kilodalton, MASH: metabolic dysfunction-associated steatohepatitis.

Western blot reveals EV marker expression – To confirm the presence of different EV surface markers and assess potential contamination in SEC-isolated fractions, western blotting was performed on a representative MASH liver sample collected after 25 weeks of dietary intervention (Fig. 6). EV-enriched markers CD63, CD81 and Alix were detected predominantly in fractions seven to ten, while CD9 was absent. Notably, the lipoprotein marker ApoE was detected in the liver cell lysate and in fractions eight to ten. Furthermore, the apoptosis-related protein BAX was not detected in both the cell lysate and the SEC-isolated fraction.

EVs from MASH livers affect BBB integrity – TEER was used to evaluate barrier integrity in hCMEC/D3 cells, a cell line that resembles the human BBB endothelial cells, after treatment with EVs isolated from control and MASH livers at different weeks on the diet. No significant differences were observed, but EVs from 25-week MASH samples showed an apparent decrease in TEER, suggesting reduced barrier function (Fig. 7). This effect was less apparent at earlier timepoints or in control conditions, indicating that EVs from fully developed MASH may contribute to BBB dysfunction.

Flow cytometry suggests subtle changes in endothelial adhesion and activation upon MASH EV exposure – To assess potential EV-induced alterations in endothelial surface marker expression, hCMEC/D3 cells were incubated with EVs and subsequently analysed using flow cytometry. Expression of ICAM-1, measured by median fluorescence intensity (MFI), appeared slightly elevated in MASH EV-treated conditions compared to control, although not statistically significant (Fig. 8A, Fig. S3A, Fig. S4).

A similar trend was observed for VCAM-1, with a notably higher expression in the 25-week MASH EV condition, suggesting possible endothelial activation in response to MASH liver-derived EVs (Fig. 8B, Fig. S3B, Fig. S4). In contrast, VE-Cadherin, a key endothelial junctional protein, showed a downward trend across MASH conditions, with 25-week MASH EVs eliciting a visibly lower expression compared to control (Fig. 78, Fig. S3C, Fig. S4). This may reflect EV-induced disruption of endothelial integrity, in line with barrier-modulating effects observed in other assays. Collectively, while changes were not statistically significant, the data indicate a possible MASH-dependent modulation of adhesion and junction markers in BBB endothelial cells.

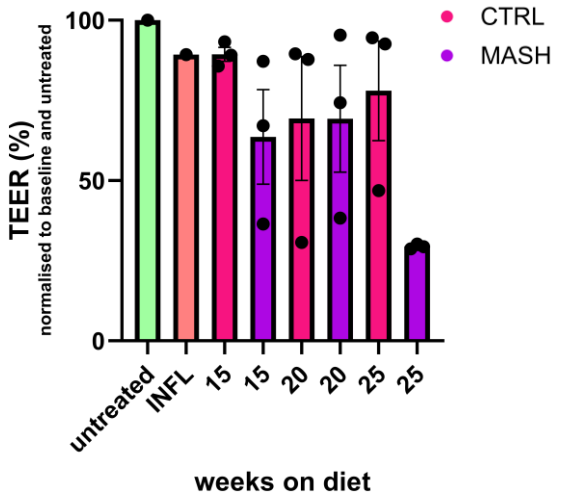

Fig. 7 – TEER analysis indicates impaired BBB integrity following exposure to MASH-derived liver EVs.
TEER was measured over a hCMEC/D3 monolayer after treatment with fraction four of SEC-isolated EVs from livers of mice on CTRL or MASH-inducing diets for 15, 20, or 25 weeks. TEER values are normalized to baseline and respective CTRL conditions. A Kruskal-Wallis test was performed, n=1 for untreated and INFL (TNF-α + INF- γ) n=3 for all CTRL and MASH time points, the data are presented as mean ± SEM.
BBB: blood-brain barrier, CTRL: control, hCMEC/D3: human cerebral microvascular endothelial cell line, INFL: inflammation, MASH: metabolic dysfunction-associated steatohepatitis, TEER: transendothelial electrical resistance.

DISCUSSION

Recent studies have described the adverse effects of MASH on the integrity of the BBB, with dysfunction primarily attributed to the disruption of endothelial junctional complexes (18, 20, 23, 24). However, the exact mechanisms underlying BBB impairment in the context of MASH remain elusive. Building upon this foundation, we propose a novel hypothesis in which liver-derived EVs act as key mediators of inter-organ communication that disrupt the structural integrity of the BBB and consequently impair its function. Specifically, we hypothesized that these EVs increasingly contribute to BBB disruption as MASH progresses, particularly at more advanced disease stages.

Mice fed the GAN diet for 15, 20, or 25 weeks developed hallmark features of MASH, including hepatomegaly and increased total body weight, consistent with previous findings (37-40). The observed increase in liver weight in MASH mice, compared to controls, is likely attributable to hepatic steatosis, inflammation, and hepatocytes ballooning; all hallmarks commonly associated with MASH progression (6). Particularly at 25 weeks on the diet, MASH seem to have fully developed. Moreover, the GAN diet has been shown to closely represent human MASH, with high translational relevance due to its metabolic and histopathological parallels (38).

Analysis of adipose tissue revealed a significant increase in scAT at 25 weeks, while vAT remained unchanged. vAT expansion is shown to induce a pro-inflammatory environment due to its ability to produce cytokines like TNF-α, IL-6, and IL-1β, and has been linked to neuroinflammation (41-44). The absence of significant vAT expansion suggests that BBB effects are more likely attributed to liver-derived factors rather than systemic inflammation. scAT, on the other hand, is more influenced by estrogen in female mice and tends to be less pro-inflammatory, suggesting that its expansion is less likely to confound the observed effects on BBB integrity (45).

First, the effects of MASH on the BBB should be studied. Therefore, qPCR analysis was utilized to determine the effects of MASH on different markers in the brain, more specifically, markers associated with the junctional complexes, leukocyte adhesion, and inflammation. Expression of CLDN5 and ZO-1 showed a very small downward trend at 25 weeks, indicating potential weakening of tight junctional expression, indicative of increasing BBB permeability. VCAM-1 and ICAM-1, both key mediators of leukocyte adhesion at the BBB, appear modestly upregulated at later weeks, with a more pronounced response observed for VCAM-1, a trend that aligns with findings from a previous study (24). The increased expression of these molecules suggests a heightened endothelial activation state, which facilitates leukocyte infiltration into the CNS. This could contribute to a pro-inflammatory environment and play a role in the development of neuroinflammation and BBB breakdown. Moreover, an upregulation of CXCL10, NLRP3, and iNOS was observed. CXCL10 is a chemokine that attracts activated T cells and is often elevated in inflammatory CNS conditions (46). Its increased expression may further amplify leukocyte recruitment and contribute to the propagation of local inflammation at the BBB. Moreover, NLRP3 is a central component of the inflammasome complex; its upregulation may indicate activation of innate immune pathways and suggest that MASH-derived EVs could trigger inflammasome-mediated signalling in BBB endothelial cells, potentially driving further BBB dysfunction (47, 48). Lastly, iNOS is commonly used as a marker of microglial activation and neuroinflammation, therefore its upregulation reflects inflammatory changes within the brain parenchyma rather than directly mediating endothelial damage (49).

Next, immunohistochemistry was used to assess BBB leakage using IgG staining and blood vessel structure using laminin. IgG is a large serum protein that typically cannot cross the BBB; its presence in the brain parenchyma is indicative of barrier disruption (50). This analysis showed a progressive increase in IgG signal, with the most pronounced leakage observed at 25 weeks. This suggests increased permeability, potentially allowing infiltration of leukocytes, toxins, and other circulating factors into the CNS. Such leakage may

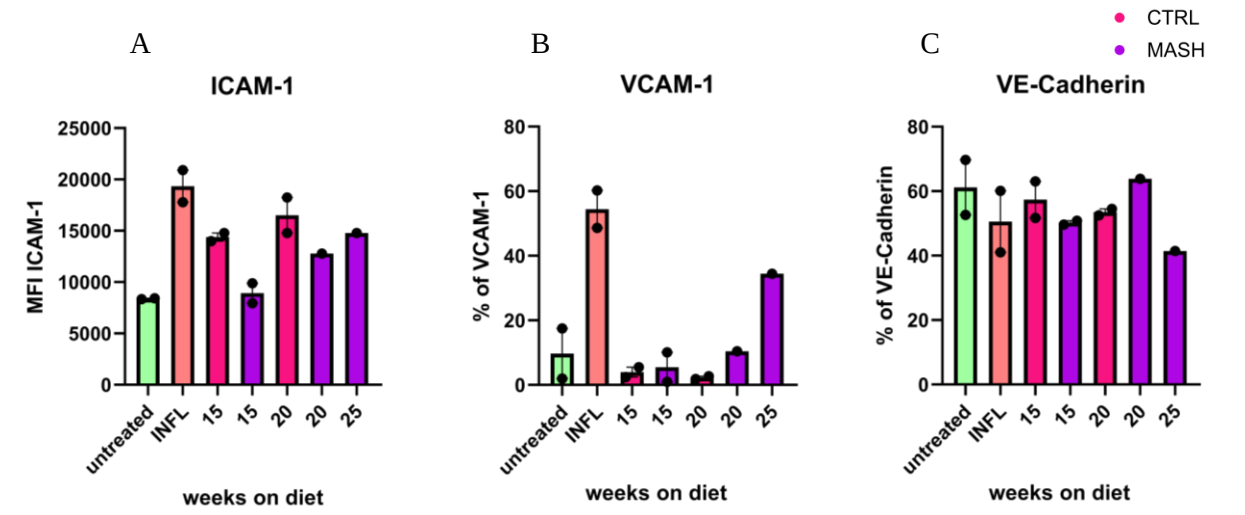

Fig. 8 – **MASH EVs modulate leukocyte adhesion and adherens junctions of the BBB.** hCMEC/D3 cells were treated with fraction four SEC-isolated EVs from livers of CTRL or MASH mice (15, 20, or 25 weeks on diet), and expression of ICAM-1 (MFI), VCAM-1 (% positive cells), and VE-Cadherin (% positive cells) was assessed by flow cytometry. A Kruskal-Wallis test was performed, n = 2 for all groups, except 25-week MASH (n = 1); the data are presented as mean ± SEM.
CTRL: control, MASH: metabolic dysfunction-associated steatohepatitis, ICAM-1: intercellular adhesion molecule 1, VCAM-1: vascular cell adhesion molecule 1, VE-Cadherin: vascular endothelial Cadherin, MFI: median fluorescence intensity, BBB: blood-brain barrier.

contribute to neuroinflammation and neural injury (51).

Given that the GAN diet successfully induced MASH, which was associated with impaired BBB integrity, EVs from both pathological and non-pathological livers can now be investigated to characterize their properties and assess their potential impact on the BBB. Therefore, EVs were isolated from liver-conditioned medium using SEC, which is a method for isolating vesicles based on size with high purity (25). Larger particles elute earlier, while smaller proteins and contaminants elute later, which was also visualized by BCA. Fraction four consistently showed the highest particle concentration according to the NTA results, making it the optimal choice for downstream analysis.

NTA confirmed the presence of vesicles in the expected size range (~123 nm), consistent with small EVs. Additionally, there was a relatively high yield, and the protein concentrations across the different SEC-isolated fractions were consistent with our expectations, thereby validating the effectiveness of SEC as an EV isolation technique (25). Moreover, western blot analysis was supposed to further characterize these isolated particles. CD9, CD63, and CD81, members of the tetraspanin family, were used as canonical exosome markers (27). Tetraspanins are integral membrane proteins commonly found on the surface of EVs and are involved in vesicle formation and cell targeting (27). Alix, a protein involved in endosomal sorting and exosome biogenesis, was also detected (27). The western blot results did not fully align with the NTA and BCA findings, as EV surface markers were predominantly detected in fractions seven to ten, rather than peaking in the earlier fractions as typically expected. This discrepancy may stem from technical variability during SEC processing. Inconsistencies in column performance or handling could have caused shifts in the elution profile, resulting in EV-containing fractions appearing later than expected. However, given that NTA and BCA data were consistent and aligned with each other, this explanation seems less likely. A more plausible cause is the partial rupture of EV membranes during sample preparation or storage, leading to the formation of aggregates that still contain EV surface markers. Due to the small size of proteins and debris, these aggregates would elute in later SEC fractions and, if present in high quantities, produce stronger signals on the western blot. This could mask the presence of intact EVs in earlier fractions, such as fractions four and five, which is more consistent with the particle and protein profiles observed by NTA and BCA. In contrast, ApoE, a lipid transport protein, was detected in the cell lysate and in fractions eight to ten, but not in fraction four. As fraction four was used for downstream analyses, this suggests it is not contaminated with lipoproteins, supporting the purity of the isolated EVs. BAX, a pro-apoptotic mitochondrial protein, was absent, suggesting no contamination with apoptotic bodies. Additionally, it is well recognized that not every EV will express all tetraspanin markers; their expression can vary depending on vesicle origin, size, and biogenesis pathway (52, 53). This heterogeneity underscores the importance of using multiple markers for EV characterization. Additionally, due to the average size of the EVs, the size distribution, and the presence of the tetraspanins, it is highly likely that the isolated EVs are predominantly exosomes (25, 27).

Now that the EVs had been characterized in terms of size, concentration, and marker expression, their potential effects on BBB integrity could be explored using functional assays. Consequently, the functional effect of MASH-derived EVs on the BBB was evaluated using TEER. TEER measures ionic resistance across an endothelial monolayer at a specific frequency, we used 1 kHz, which is optimal for assessing barrier tightness (54). A drop in resistance indicates a loss of barrier integrity due to increased paracellular permeability (54). Although changes were not statistically significant, EVs derived from MASH livers after 25 weeks on the diet consistently caused the most pronounced drop in TEER, further supporting the idea that fully developed MASH generates EVs capable of impairing BBB function.

Finally, flow cytometry was employed to assess the surface expression of endothelial adhesion and junctional proteins. ICAM-1 expression showed a mild, non-significant increase across all time points. Interestingly, VCAM-1 expression was elevated following treatment with 25-week MASH liver-derived EVs, a trend that

aligns with its known upregulation in inflammatory states and has been reported in MASH-related endothelial dysfunction (24). VE-Cadherin showed a slight decrease with MASH EV treatment at 25 weeks, supporting the TEER findings and suggesting structural weakening of the endothelial monolayer.

Importantly, the 25-week timepoint appeared to represent a critical phase in disease progression, where the cumulative stress of prolonged MASH more clearly manifested in impairment of the BBB. Taken together, our findings support the hypothesis that EVs derived from MASH livers can compromise BBB structure and function, particularly at later disease stages. While most results were not statistically significant due to sample size limitations, consistent trends across multiple experimental modalities suggest that EVs may play a crucial role in inter-organ crosstalk between the liver and brain. Future studies should focus on validating these findings in expanded cohorts, characterizing EV cargo, and tracing their systemic distribution to fully elucidate their role in MASH-related neuropathology.

While this study provides novel insights into the potential role of liver-derived EVs in mediating BBB dysfunction during MASH, several limitations must be acknowledged. First, although strong trends were observed across various readouts, many findings did not reach statistical significance, largely due to the limited sample sizes. Increasing the number of biological replicates would enhance statistical power and allow for more definitive conclusions.

Another limitation is the lack of EV tracking or detection in peripheral blood. While this study focuses on EVs derived from whole liver-conditioned media, confirmation that these EVs reach and interact with the BBB endothelium *in vivo* is crucial. Future studies should incorporate EV labelling and biodistribution experiments to visualize their systemic transport and uptake by BBB-associated cells, especially in the context of MASH. However, previous studies have shown that EVs are able to travel through the bloodstream, interact with the BBB, and can be taken up by the BBB (34, 35, 55, 56).

Furthermore, the GAN diet was administered for up to 25 weeks, which may be relatively short compared to human disease progression. Previous research employing longer dietary interventions (34 - 88 weeks) has demonstrated a more advanced and stable disease phenotype, which could more accurately reflect MASH closer to the human situation (38-40).

From a technical standpoint, while SEC is a widely accepted method for EV isolation, overlapping elution of EVs and co-isolated protein aggregates remains a concern. Therefore, additional orthogonal validation (e.g., transmission electron microscopy as described in the MISEV guidelines) would strengthen purity claims (25). Since western blotting revealed EV presence in later fractions, the consistency of SEC-based EV isolation should be monitored, and potentially an alternative technique, such as differential ultracentrifugation or polymer-based precipitation, could be considered (25).

Despite these limitations, the current findings highlight a compelling inter-organ communication axis in MASH liver-derived EVs and the BBB endothelium. Given the increase in BBB permeability and altered endothelial expression profiles upon MASH EV exposure, particularly at 25 weeks, these data support a pathogenic role of EVs in BBB impairment. The observed results suggest an increased permeability of the endothelium and a pro-inflammatory state, both of which are recognized contributors to neuroinflammatory cascades.

From a translational perspective, this work contributes to the growing recognition of MASH as a disease with implications beyond the liver. It underscores the importance of exploring EVs as mechanistic mediators and potential biomarkers of systemic organ dysfunction. Given that current diagnostic methods for MASH rely on invasive liver biopsy, improved characterization of circulating EVs could provide a valuable alternative for diagnosis and disease monitoring. Furthermore, targeting EV secretion, release, or uptake may represent a promising therapeutic approach to prevent BBB disruption and mitigate associated neurological complications in patients with MASH.

CONCLUSION

This study provides new perspectives on how metabolic liver disease, specifically MASH, may contribute to early neuroinflammatory changes through disruption of the BBB. The results suggest that as MASH progresses, liver-derived EVs reflect the pathological state of the liver and undergo changes that potentially impair the structural and functional integrity of the BBB. While direct causality remains to be fully established, consistent trends point toward increased endothelial activation and reduced junctional stability, features of a compromised barrier. These findings support the concept of liver–brain communication in MASH and propose a mechanistic role for EVs in mediating this inter-organ interaction. This work provides a valuable foundation for future studies aimed at understanding how peripheral organ pathology can influence CNS health and whether targeting EVs could offer novel therapeutic opportunities.

REFERENCES

1. Kalra A, Yetiskul E, Wehrle CJ, Tuma F. Physiology, Liver. StatPearls. Treasure Island (FL)2025.
2. Robinson MW, Harmon C, O'Farrelly C. Liver immunology and its role in inflammation and homeostasis. Cell Mol Immunol. 2016;13(3):267-76.
3. Krishna M. Microscopic anatomy of the liver. Clin Liver Dis (Hoboken). 2013;2(Suppl 1):S4-S7.
4. Gong J, Tu W, Liu J, Tian D. Hepatocytes: A key role in liver inflammation. Front Immunol. 2022;13:1083780.
5. Eipel C, Abshagen K, Vollmar B. Regulation of hepatic blood flow: the hepatic arterial buffer response revisited. World J Gastroenterol. 2010;16(48):6046-57.
6. Pouwels S, Sakran N, Graham Y, Leal A, Pintar T, Yang W, et al. Non-alcoholic fatty liver disease (NAFLD): a review of pathophysiology, clinical management and effects of weight loss. BMC Endocr Disord. 2022;22(1):63.
7. Rinella ME, Sookoian S. From NAFLD to MASLD: updated naming and diagnosis criteria for fatty liver disease. J Lipid Res. 2024;65(1):100485.
8. Zou X, Brigstock D. Extracellular Vesicles from Mesenchymal Stem Cells: Potential as Therapeutics in Metabolic Dysfunction-Associated Steatotic Liver Disease (MASLD). Biomedicines. 2024;12(12).
9. Rinella ME, Lazarus JV, Ratziu V, Francque SM, Sanyal AJ, Kanwal F, et al. A multisociety Delphi consensus statement on new fatty liver disease nomenclature. J Hepatol. 2023;79(6):1542-56.
10. van Son KC, Te Nijenhuis-Noort LC, Boone SC, Mook-Kanamori DO, Holleboom AG, Roos PR, et al. Prevalence of metabolic dysfunction-associated steatotic liver disease (MASLD) in a middle-aged population with overweight and normal liver enzymes, and diagnostic accuracy of noninvasive proxies. Medicine (Baltimore). 2024;103(1):e34934.
11. Li Y, Yang P, Ye J, Xu Q, Wu J, Wang Y. Updated mechanisms of MASLD pathogenesis. Lipids Health Dis. 2024;23(1):117.
12. Younossi ZM. The epidemiology of nonalcoholic steatohepatitis. Clin Liver Dis (Hoboken). 2018;11(4):92-4.
13. Fan W, Bradford TM, Torok NJ. Metabolic dysfunction-associated liver disease and diabetes: Matrix remodeling, fibrosis, and therapeutic implications. Ann N Y Acad Sci. 2024;1538(1):21-33.
14. Seen TK, Sayed M, Bilal M, Reyes JV, Bhandari P, Lourdusamy V, et al. Clinical indicators for progression of nonalcoholic steatohepatitis to cirrhosis. World J Gastroenterol. 2021;27(23):3238-48.

15. Kawanaka M, Nishino K, Morimoto Y, Ishii K, Tanikawa T, Urata N, et al. Progression from Nonalcoholic Fatty Liver to Nonalcoholic Steatohepatitis Cirrhosis Confirmed by Liver Histology after 14 Years. Intern Med. 2021;60(9):1397-401.
16. Schuster S, Cabrera D, Arrese M, Feldstein AE. Triggering and resolution of inflammation in NASH. Nat Rev Gastroenterol Hepatol. 2018;15(6):349-64.
17. Li YY, Zheng TL, Xiao SY, Wang P, Yang WJ, Jiang LL, et al. Hepatocytic ballooning in non-alcoholic steatohepatitis: Dilemmas and future directions. Liver Int. 2023;43(6):1170-82.
18. Mondal A, Bose D, Saha P, Sarkar S, Seth R, Kimono D, et al. Lipocalin 2 induces neuroinflammation and blood-brain barrier dysfunction through liver-brain axis in murine model of nonalcoholic steatohepatitis. J Neuroinflammation. 2020;17(1):201.
19. Fiaschini N, Mancuso M, Tanori M, Colantoni E, Vitali R, Diretto G, et al. Liver Steatosis and Steatohepatitis Alter Bile Acid Receptors in Brain and Induce Neuroinflammation: A Contribution of Circulating Bile Acids and Blood-Brain Barrier. Int J Mol Sci. 2022;23(22).
20. Mondal A, Saha P, Bose D, Chatterjee S, Seth RK, Xiao S, et al. Environmental Microcystin exposure in underlying NAFLD-induced exacerbation of neuroinflammation, blood-brain barrier dysfunction, and neurodegeneration are NLRP3 and S100B dependent. Toxicology. 2021;461:152901.
21. Schreiner TG, Romanescu C, Popescu BO. The Blood-Brain Barrier-A Key Player in Multiple Sclerosis Disease Mechanisms. Biomolecules. 2022;12(4).
22. Feng Z, Fang C, Ma Y, Chang J. Obesity-induced blood-brain barrier dysfunction: phenotypes and mechanisms. J Neuroinflammation. 2024;21(1):110.
23. Giuffre M, Merli N, Pugliatti M, Moretti R. The Metabolic Impact of Nonalcoholic Fatty Liver Disease on Cognitive Dysfunction: A Comprehensive Clinical and Pathophysiological Review. Int J Mol Sci. 2024;25(6).
24. Furuta K, Guo Q, Pavelko KD, Lee JH, Robertson KD, Nakao Y, et al. Lipid-induced endothelial vascular cell adhesion molecule 1 promotes nonalcoholic steatohepatitis pathogenesis. J Clin Invest. 2021;131(6).
25. Welsh JA, Goberdhan DCI, O'Driscoll L, Buzas EI, Blenkiron C, Bussolati B, et al. Minimal information for studies of extracellular vesicles (MISEV2023): From basic to advanced approaches. J Extracell Vesicles. 2024;13(2):e12404.
26. Liu YJ, Wang C. A review of the regulatory mechanisms of extracellular vesicles-mediated intercellular communication. Cell Commun Signal. 2023;21(1):77.
27. Andreu Z, Yanez-Mo M. Tetraspanins in extracellular vesicle formation and function. Front Immunol. 2014;5:442.
28. Dorairaj V, Sulaiman SA, Abu N, Abdul Murad NA. Extracellular Vesicles in the Development of the Non-Alcoholic Fatty Liver Disease: An Update. Biomolecules. 2020;10(11).
29. Kumar V, Kiran S, Kumar S, Singh UP. Extracellular vesicles in obesity and its associated inflammation. Int Rev Immunol. 2022;41(1):30-44.
30. Kranendonk ME, Visseren FL, van Herwaarden JA, Nolte-'t Hoen EN, de Jager W, Wauben MH, et al. Effect of extracellular vesicles of human adipose tissue on insulin signaling in liver and muscle cells. Obesity (Silver Spring). 2014;22(10):2216-23.
31. Connolly KD, Guschina IA, Yeung V, Clayton A, Draman MS, Von Ruhland C, et al. Characterisation of adipocyte-derived extracellular vesicles released pre- and post-adipogenesis. J Extracell Vesicles. 2015;4:29159.

32. Wang Q, Tang X, Wang Y, Zhang D, Li X, Liu S. The role of extracellular vesicles in non-alcoholic steatohepatitis: Emerging mechanisms, potential therapeutics and biomarkers. J Adv Res. 2025;69:157-68.
33. Ipsen DH, Tveden-Nyborg P. Extracellular Vesicles as Drivers of Non-Alcoholic Fatty Liver Disease: Small Particles with Big Impact. Biomedicines. 2021;9(1).
34. Ramos-Zaldivar HM, Polakovicova I, Salas-Huenuleo E, Corvalan AH, Kogan MJ, Yefi CP, et al. Extracellular vesicles through the blood-brain barrier: a review. Fluids Barriers CNS. 2022;19(1):60.
35. Hosseinkhani B, Duran G, Hoeks C, Hermans D, Schepers M, Baeten P, et al. Cerebral microvascular endothelial cell-derived extracellular vesicles regulate blood - brain barrier function. Fluids Barriers CNS. 2023;20(1):95.
36. Busatto S, Morad G, Guo P, Moses MA. The role of extracellular vesicles in the physiological and pathological regulation of the blood-brain barrier. FASEB Bioadv. 2021;3(9):665-75.
37. Saenz M, McDonough JC, Bloom-Saldana E, Irimia JM, Cauble EL, Castillo A, et al. Longitudinal analysis of a dietary mouse model of non-alcoholic fatty liver disease (NAFLD) and non-alcoholic steatohepatitis (NASH). bioRxiv. 2023.
38. Hansen HH, HM AE, Oro D, Evers SS, Heeboll S, Eriksen PL, et al. Human translatability of the GAN diet-induced obese mouse model of non-alcoholic steatohepatitis. BMC Gastroenterol. 2020;20(1):210.
39. Flensted-Jensen M, Oro D, Rorbeck EA, Zhang C, Madsen MR, Madsen AN, et al. Dietary intervention reverses molecular markers of hepatocellular senescence in the GAN diet-induced obese and biopsy-confirmed mouse model of NASH. BMC Gastroenterol. 2024;24(1):59.
40. Mollerhoj MB, Veidal SS, Thrane KT, Oro D, Overgaard A, Salinas CG, et al. Hepatoprotective effects of semaglutide, lanifibranor and dietary intervention in the GAN diet-induced obese and biopsy-confirmed mouse model of NASH. Clin Transl Sci. 2022;15(5):1167-86.
41. Park HS, Park JY, Yu R. Relationship of obesity and visceral adiposity with serum concentrations of CRP, TNF-alpha and IL-6. Diabetes Res Clin Pract. 2005;69(1):29-35.
42. Macdougall CE, Wood EG, Loschko J, Scagliotti V, Cassidy FC, Robinson ME, et al. Visceral Adipose Tissue Immune Homeostasis Is Regulated by the Crosstalk between Adipocytes and Dendritic Cell Subsets. Cell Metab. 2018;27(3):588-601 e4.
43. Ghanbari M, Momen Maragheh S, Aghazadeh A, Mehrjuyan SR, Hussen BM, Abdoli Shadbad M, et al. Interleukin-1 in obesity-related low-grade inflammation: From molecular mechanisms to therapeutic strategies. Int Immunopharmacol. 2021;96:107765.
44. de ABAP, de OCPH, BE FF, PS ES, de Moraes L, Migliolo L. Adipose tissue, systematic inflammation, and neurodegenerative diseases. Neural Regen Res. 2023;18(1):38-46.
45. Gavin KM, Bessesen DH. Sex Differences in Adipose Tissue Function. Endocrinol Metab Clin North Am. 2020;49(2):215-28.
46. Trevino TN, Almousawi AA, Martins-Goncalves R, Ochoa-Raya A, Robinson KF, Abad GL, et al. A Brain Endothelial Cell Caveolin-1/CXCL10 Axis Promotes T Cell Transcellular Migration Across the Blood-Brain Barrier. ASN Neuro. 2025;17(1):2472070.
47. Swanson KV, Deng M, Ting JP. The NLRP3 inflammasome: molecular activation and regulation to therapeutics. Nat Rev Immunol. 2019;19(8):477-89.

48. Yoon SH, Kim CY, Lee E, Lee C, Lee KS, Lee J, et al. Microglial NLRP3-gasdermin D activation impairs blood-brain barrier integrity through interleukin-1beta-independent neutrophil chemotaxis upon peripheral inflammation in mice. Nat Commun. 2025;16(1):699.
49. Saha RN, Pahan K. Regulation of inducible nitric oxide synthase gene in glial cells. Antioxid Redox Signal. 2006;8(5-6):929-47.
50. Goldwaser EL, Swanson RL, 2nd, Arroyo EJ, Venkataraman V, Kosciuk MC, Nagele RG, et al. A Preliminary Report: The Hippocampus and Surrounding Temporal Cortex of Patients With Schizophrenia Have Impaired Blood-Brain Barrier. Front Hum Neurosci. 2022;16:836980.
51. Takata F, Nakagawa S, Matsumoto J, Dohgu S. Blood-Brain Barrier Dysfunction Amplifies the Development of Neuroinflammation: Understanding of Cellular Events in Brain Microvascular Endothelial Cells for Prevention and Treatment of BBB Dysfunction. Front Cell Neurosci. 2021;15:661838.
52. Jeppesen DK, Fenix AM, Franklin JL, Higginbotham JN, Zhang Q, Zimmerman LJ, et al. Reassessment of Exosome Composition. Cell. 2019;177(2):428-45 e18.
53. Barranco I, Padilla L, Parrilla I, Alvarez-Barrientos A, Perez-Patino C, Pena FJ, et al. Extracellular vesicles isolated from porcine seminal plasma exhibit different tetraspanin expression profiles. Sci Rep. 2019;9(1):11584.
54. Srinivasan B, Kolli AR, Esch MB, Abaci HE, Shuler ML, Hickman JJ. TEER measurement techniques for in vitro barrier model systems. J Lab Autom. 2015;20(2):107-26.
55. Shi M, Sheng L, Stewart T, Zabetian CP, Zhang J. New windows into the brain: Central nervous system-derived extracellular vesicles in blood. Prog Neurobiol. 2019;175:96-106.
56. Povero D, Yamashita H, Ren W, Subramanian MG, Myers RP, Eguchi A, et al. Characterization and Proteome of Circulating Extracellular Vesicles as Potential Biomarkers for NASH. Hepatol Commun. 2020;4(9):1263-78.

Acknowledgements – I would like to sincerely thank Daphne Lintsen for her invaluable guidance, support, and feedback throughout my internship. Her mentorship was essential to the completion of this project. I am also grateful to Prof. Dr. Broux and the entire CBN team for their insightful feedback, collaborative spirit, and the many learning opportunities they provided during my time in the lab. Special thanks go to Prof. Dr. Kristiaan Wouters and Dr. Sabine Daemen from Maastricht University for kindly providing the liver tissue that was essential for this research.

Author contributions – DL and BB conceived and designed the research. CM and DL performed experiments and data analysis. CM wrote the paper with the assistance of DL. All authors carefully edited the manuscript. GenAI was used for grammatical and linguistic support.

Supporting information

Supplementary methods

BCA – To quantify protein concentrations, the bicinchoninic acid (BCA) protein assay kit (ThermoFisher, USA) was utilized according to the manufacturer's instructions. The absorbance was measured at 562 nm at 37°C using a CLARIOstar plus spectrophotometer (BMG labtech, Germany). Samples were measured *in duplo*.

Supplementary table 1 – qPCR primers

Target	Forward primer	Reverse primer
ZO-1	GGCATTCCTGCTGGTTACA	AGGACACCAAAGCATGTGAG
CLDN5	GTCAAGGTAACAAAGAGTGCCA	GCAAGGTGTATGAATCTGTGCT
VE-Cadherin	GTGTTAGCATCGACCCCGAA	CCAACGTGAACCGCCAGAA
VCAM-1	CCTTGTGGAGGGATGTACAGA	TGCCGAGCTAAATTACACATTG
ICAM-1	GACCGGAGCTGAAAAGTTGTA	GCCTTGGTAGAGGTGACTGAG
CXCL10	GCCTATCGCCAATGAGCTG	CTGAACCAAGGGAGCTTCAGG
iNOS	CCCTTCAATGGTTGGTACATGG	ACATTGATCTCCGTGACAGCC
NLRP3	AATACCCGCCCGAGAAAG	TCGCAGCAAAGATCCACACAG

Supplementary results

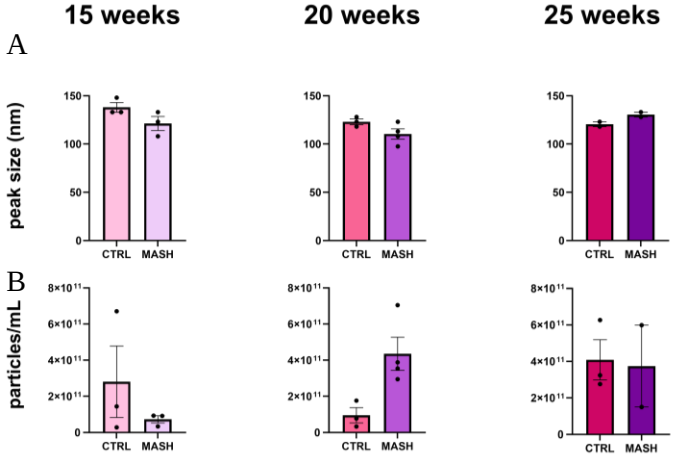

Fig. S1 – NTA shows no significant differences in peak size of particles and particle concentration in fraction four of CTRL and MASH.

Peak size of the EVs across different diet durations (A). Total EV particle concentrations in fraction four across different weeks on the diet (B). Statistical analysis by Mann-Whitney U test, n = 3/group, data presented as mean ± SEM.

CTRL: control, MASH: metabolic dysfunction-associated steatohepatitis, NTA: nanoparticle tracking analysis.

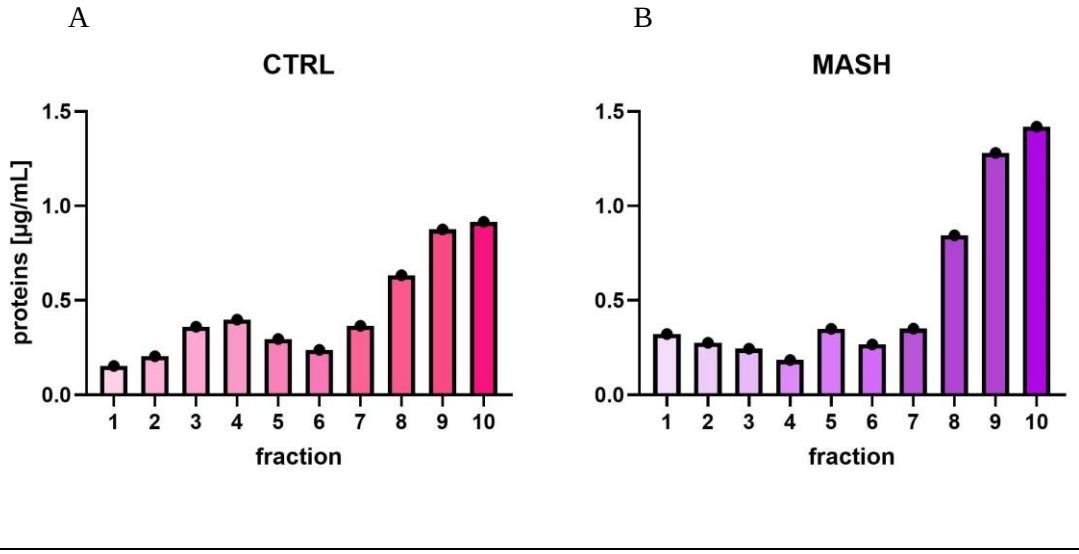

Fig. S2 – **Protein concentrations increase across SEC fractions in CTRL and MASH liver-derived samples of 20 weeks.**
BCA assay of 10 sequential SEC fractions collected from CTRL (A) and MASH (B) liver-derived samples. n=1.
BCA: bicinchoninic acid, CTRL: control, MASH: metabolic dysfunction-associated steatohepatitis, SEC: size-exclusion chromatography.

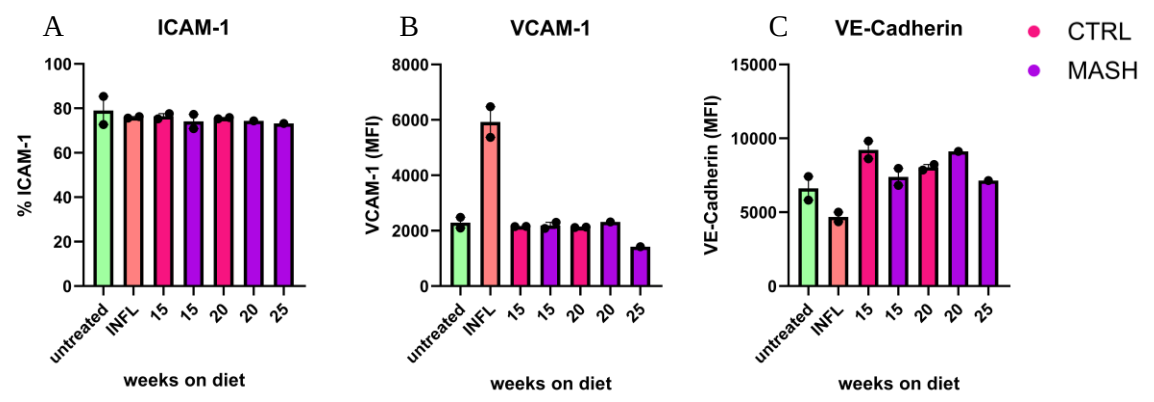

Fig. S3 – **MASH EVs modulate leukocyte adhesion and junctional complexes of the BBB.**
hCMEC/D3 cells were treated with fraction four SEC-isolated EVs from livers of CTRL or MASH mice (15, 20, or 25 weeks on diet), and expression of ICAM-1 (% positive cells), VCAM-1 (MFI), and VE-Cadherin (MFI) was assessed by flow cytometry. Data were normalized to CTRL-treated cells. A Kruskal-Wallis test was performed, n = 2 for all groups, except 25-week MASH (n = 1); the data are presented as mean ± SEM.
BBB: blood-brain barrier, CTRL: control, ICAM-1: intercellular adhesion molecule 1, MASH: metabolic dysfunction-associated steatohepatitis, MFI: median fluorescence intensity, VE-Cadherin: vascular endothelial Cadherin, VCAM-1: vascular cell adhesion molecule 1.

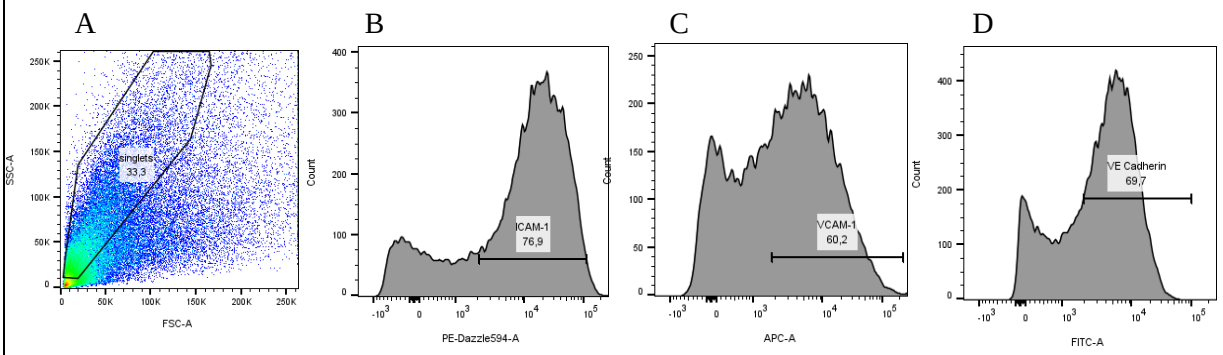

Fig. S4 – Gating for EVs treatment of hCMEC/D3 cells. hCMEC/D3 cells were treated with TNF-α + INF-γ. Gating was performed in FlowJo.
ICAM-1: intercellular adhesion molecule 1, VCAM-1: vascular cell adhesion molecule 1, VE-Cadherin: vascular endothelial Cadherin.